On the Time-Domain Response of Havriliak-Negami Dielectrics

Matthew F. Causley, Peter G. Petropoulos

***Abstract*—We apply a combination of asymptotic and numerical methods to study electromagnetic pulse propagation in the Havriliak-Negami permittivity model of fractional relaxation. This dielectric model contains the Cole-Cole and Cole-Davidson models as special cases. We analytically determine the impulse response at short and long distances behind the wavefront, and validate our results with numerical methods for performing inverse Laplace transforms and for directly solving the time-domain Maxwell equations in such dielectrics. We find that the time-domain response of Havriliak-Negami dielectrics is significantly different from that obtained for Debye dielectrics. This makes possible using pulse propagation measurements in TDR setups in order to determine the appropriate dielectric model, and its parameters, for the actual dielectric whose properties are being measured.**

***Index Terms*—Havriliak-Negami dielectric model, Fractional relaxation, Debye dielectric model, dispersive dielectrics, Maxwell equations, Time-domain.**

I. Introduction

Previous work [1]-[2]-[3]-[4] on the asymptotics of pulse propagation in the Debye model [5] of induced macroscopic electric polarization has been shown [6] to agree with published laboratory measurements [7] obtained using pulses and geometries typically found in the Time-Domain Reflectometry (TDR) method for the determination of the frequency-dependent dielectric properties of materials. More recent work [8] independently verifies all the aforementioned theoretical and experimental results. Significantly, the large-depth time-domain response of a Debye dielectric satisfies an advection-diffusion equation and thus it is symmetric about its peak which is found on a sub-characteristic ray whose speed is a fraction of the speed of light in such materials [1]-[2].

M. F. Causley is with the Department of Mathematics, Michigan State University, East Lansing, MI 48824 (causleym@msu.edu).

P. G. Petropoulos is with the Department of Mathematical Sciences, New Jersey Institute of Technology, Newark, NJ 07102 (peterp@njit.edu).

Manuscript received August 14, 2012; revised January XX, XXXX.

There is a large class of materials whose microstructure yields an induced macroscopic electric polarization that is markedly different from that of the Debye kind. A small sample of materials in this class includes: amorphous polymers near glassy phase transition [9],[10]; heterogeneous soils [11]; and, perhaps most importantly, the various complex biological tissues in the human body [12]-[13]-[14]. The experimentally-measured time-domain responses in [15] indicate that in such materials it is non-symmetric responses, which are not characteristic of propagation in a Debye dielectric, that are prevalent (Section 4.4 of [15]). On the basis of our previous work [16], where we determined that the time-domain response of the Cole-Cole dielectric model is non-symmetric about its peak value, it appears evident that for such materials a hierarchy of empirical models for the induced macroscopic electric polarization, which we will refer to as Fractional Relaxation Models (FRMs), is more appropriate. Such empirical models have been developed over the last 70 years and include: the Cole-Cole (C-C) model [17], the Cole-Davidson (C-D) model [18], and the Havriliak-Negami (H-N) model [19]. While FRMs have been introduced as purely empirical models, recent work [20] derives such models from first principles and interprets the fractional relaxation they introduce as the interaction of different polarizable species with many different dielectric moments. Consequently, a distribution of relaxation times that peaks at some characteristic value τ is present, and it is the shape of this distribution function which gives rise to the various FRMs. In the time domain, these FRMs introduce non-exponential electric susceptibilities which are algebraically decaying in time and are singular as $t \to 0^+$.

Previously, we have examined the asymptotics of electromagnetic pulse propagation in the Cole-Cole dielectric model [16] and identified an open problem which we resolve in the present paper. Also, we

have developed an algorithm to incorporate the H-N model in the FDTD method [21] in a way that allows the calculation of the time-dependent impulse response of an H-N dielectric target with a preset error. In our asymptotic and numerical FRM-related work we have determined that propagated pulses in such dielectric models evolve to non-symmetric shapes which are distinct from the shapes obtained when dielectrics are represented with the Debye medium model. This lends credence to the suggestion that FRMs may be more appropriate for representing the dielectric permittivity data obtained experimentally for complex media beyond water.

The present work aims to complete our contributions to the numerical and asymptotic study of pulse propagation in anomalously dispersive lossy dielectric models by presenting an asymptotic analysis of pulse propagation in the H-N model, which is the most general of the known FRMs. The frequency-dependent relative permittivity, which now involves two fractional parameters α and β, where $0 < \alpha, \beta < 1$, is given by

$$\epsilon(s)/\epsilon_0 = \epsilon_\infty + \frac{\epsilon_s - \epsilon_\infty}{(1+(s\tau)^\alpha)^\beta}, \tag{1}$$

where $s = i\omega$ is the complex frequency (below we will work with the Laplace transform), ϵ_s and ϵ_∞ are respectively the zero- and infinite-frequency limits of the relative permittivity, ϵ_0 is the permittivity of vacuum, and τ is the relaxation time at which the distribution of relaxation times achieves its peak. The Debye model is the special case $\alpha = \beta = 1$, while the Cole-Cole model is obtained when $0 < \alpha < 1,\ \beta = 1$, and the Cole-Davidson model is obtained when $\alpha = 1,\ 0 < \beta < 1$. We derive the time-domain Green's function for the H-N medium, and study it with asymptotic methods valid for short and large depths. Our model problem emulates a signaling problem in the TDR setup and is described in Section II, where the exact evaluation of the model's solution is also discussed. The asymptotic results for short- and large-depth behavior are constructed and validated in Section III. In Section IV we investigate the possibility of using our analytical/numerical results for model parameter estimation using experimentally-obtained data (simulated herein with our FDTD code [21]) on propagated pulses such as those encountered during TDR measurements. Also, we connect our analysis to pulse propagation in lossless random media whose properties exhibit short- or long-range correlations thus creating the possibility of using TDR-measured responses to probe the statistics of the microstructure of complex dielectrics.

II. Model Equations and their Exact Solution

We consider, with the geometry of TDR in mind, a pulsed plane-wave propagating through a one-dimensional non-magnetic ($\mu = \mu_0$) dielectric half-space $x > 0$ whose permittivity is modeled with (1). The time-domain Maxwell's equations reduce to

$$\frac{\partial^2}{\partial t^2}\left(\epsilon_0\epsilon_\infty E + P\right) = \frac{1}{\mu_0}\frac{\partial^2 E}{\partial x^2}, \quad t > 0, \tag{2}$$

where $E(x,t)$ is the electric field, and $P(x,t)$ is the induced electric polarization. Signaling data is prescribed at the boundary $x = 0$,

$$E(0,t) = f(t), \quad t > 0, \tag{3}$$

and $E(x,0) = 0$ for $x > 0$. The induced electric polarization is defined to be

$$P = \epsilon_0 \int_0^t \chi(t-t')E(x,t')dt', \tag{4}$$

where the time-domain susceptibility, $\chi(t)$, is obtained via the inverse Laplace transform from (1) as

$$\begin{aligned}\chi(t) &= \mathcal{L}^{-1}\left\{\frac{\epsilon_s - \epsilon_\infty}{(1+(s\tau)^\alpha)^\beta}\right\} \\ &= \frac{1}{2\pi i}\int_{\zeta-i\infty}^{\zeta+i\infty}\frac{(\epsilon_s-\epsilon_\infty)e^{st}}{(1+(s\tau)^\alpha)^\beta}ds, \quad t > 0. \end{aligned} \tag{5}$$

Applying standard Laplace transform arguments reduces (2)-(5) to an ordinary differential equation for $\hat{E}(x,s) = \mathcal{L}\{E\}$,

$$\frac{\partial^2 \hat{E}}{\partial x^2} - \left(\frac{s}{c(s)}\right)^2 \hat{E} = 0, \quad x > 0, \tag{6}$$

with boundary data

$$\hat{E}(0,s) = F(s) = \mathcal{L}\left\{f(t)\right\}.$$

Defining the frequency-dependent wave speed as

$$c(s) = \frac{1}{\sqrt{\mu_0\epsilon(s)}} = \frac{c_\infty}{q(s\tau)}, \tag{7}$$

where $c_\infty = \frac{1}{\sqrt{\mu_0\epsilon_0\epsilon_\infty}}$, with

$$q(s\tau) = \sqrt{1 + \frac{r-1}{(1+(s\tau)^\alpha)^\beta}}, \quad r = \frac{\epsilon_s}{\epsilon_\infty}, \tag{8}$$

and requiring that $\hat{E}(x,s)$ is bounded as $x \to \infty$, we obtain the electric field in the half-space on and behind the wavefront as

$$E(x,t) = \mathcal{L}^{-1}\left\{F(s)\hat{\Psi}(x,s)\right\} = \frac{1}{2\pi i}\int_{\zeta-i\infty}^{\zeta+i\infty}\left[F(s)e^{-\frac{sx}{c_\infty}q(s\tau)}\right]e^{st}ds, \quad (9)$$

for $t \geq \frac{x}{c_\infty}$. Setting $F(s) = 1$ in (9) we obtain the time-domain representation of the impulse response

$$\Psi(x,t) = \int_C \exp\left(st - \frac{sx}{c_\infty}q(s\tau)\right)ds, \quad (10)$$

where C is an integration contour as in (9) or an allowable deformation of it in the complex $s-$domain.

Equation (10) will be studied asymptotically, and numerically by appropriate quadrature along C. The region of analyticity of $\hat{\Psi} = \exp\left(-\frac{sx}{c_\infty}q(s\tau)\right)$ is independent of α and β. The square root in (8) produces a branch cut along the negative real axis, and so the region of analyticity will be s for which $-\pi < \arg s < \pi$. Thus, we can define C to be any curve that begins at $s = \infty$ in the third quadrant, passes to the right of any singularities of F, and terminates at $s = \infty$ in the second quadrant. Once a suitable contour is chosen, we construct N quadrature points (w_k, s_k), where each s_k is on the contour; we then apply the mapping $s = z/t$, so that (10) is approximated as

$$\Psi(x,t) \approx \sum_{k=1}^{N}\frac{w_k}{t}\exp\left(z_k - \frac{z_k x}{c_\infty t}q(z_k\tau/t)\right). \quad (11)$$

If $F(s)$ is known, then (9) can be computed directly with this method, by replacing w_k with $w_k F(z_k/t)$. Otherwise, we can obtain $\Psi(x,t)$, and convolve it in the time domain with the signaling data, $f(t)$. The choice of contour will determine the accuracy of the approximation and the number of points N required to obtain a desired accuracy. Ideally, a steepest descent contour would be determined, which will pass through a saddle point, and along which the imaginary part of the phase $\phi = st - \frac{sx}{c_\infty}q(s\tau)$ is constant. The saddle point satisfies $d\phi/ds = 0$,

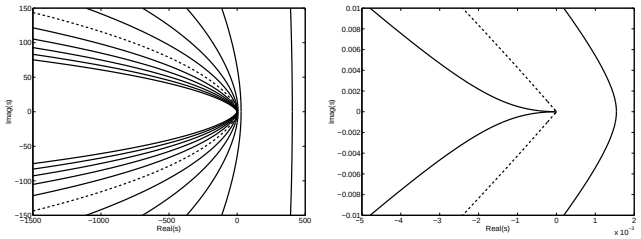

(a) Zoom-out (b) Zoom-in

Figure 1: Numerically determined steepest descent contours for the H-N impulse response. The saddle point is at the intersection of each contour with the Real$-s$ axis. The contour and saddle point move to the left as the parameter θ increases, and the saddle point moves into the origin when $\theta = \frac{c_\infty}{c_s}$ (dotted line). For $\theta > \frac{c_\infty}{c_s}$, the contour forms a cusp at the origin.

which yields the expression

$$\begin{aligned}\theta &= q(s\tau) + s\tau q'(s\tau)\\ &= q(s\tau) - \frac{\alpha\beta(s\tau)^\alpha}{2(1+(s\tau)^\alpha)}\left(\frac{(q(s\tau))^2-1)}{q(s\tau)}\right)\\ &= \frac{1+\frac{r-1}{(1+(s\tau)^\alpha)^\beta} - \frac{\alpha\beta(r-1)(s\tau)^\alpha}{2(1+(s\tau)^\alpha)^{\beta+1}}}{\sqrt{1+\frac{r-1}{(1+(s\tau)^\alpha)^\beta}}},\end{aligned} \quad (12)$$

where the space-time parameter is defined as

$$\theta = \frac{c_\infty t}{x}, \quad \theta \geq 1. \quad (13)$$

Note that the saddle point depends on x and t only through θ. Unfortunately, this unwieldy expression (12) is a nonlinear equation that can be rationalized into a (degree 4) polynomial in s^α only when $\beta = 1$; otherwise the equation is transcendental. Instead of seeking a closed form solution, we find real s that satisfies (12) using Newton's method. In terms of θ, the saddle point moves along the real line, decreasing from $s(1) = \infty$, to $s(\theta^*) = 0$, where $\theta^* = \sqrt{r} = \frac{c_\infty}{c_s}$ corresponds to the subcharacteristic ray $t = x/c_s$. The speed of this subcharacteristic ray is $c_s = \frac{1}{\sqrt{\mu_0\epsilon_0\epsilon_s}}$. For $t > x/c_s$ ($\theta > \theta^*$), no real-valued saddle point exists, and the steepest descent contour develops a cusp at the origin. This is illustrated in Figure 1 for a representative set of parameters, with x fixed and θ increasing. When the saddle point exists, the contour passes through it vertically ($\arg s = \pm\frac{\pi}{2}$). Although Figure 1 is useful

to examine, it falls short of providing a parametric representation from which the steepest descent contour can be obtained. Instead, we proceed to evaluate $\Psi(x,t)$ by choosing a hyperbolic contour, as used in [22], to perform the numerical inverse Laplace transform. This contour, given by

$$s(u) = \mu\left(1 + \sin\left(iu - a\right)\right), \quad |u| < \infty, \tag{14}$$

provides a means to construct the weights and nodes (w_k, s_k). Specifically, we set

$$\begin{cases} s_k = & \mu\left(1 + \sin\left(iu_k - a\right)\right), \\ w_k = & \frac{\mu}{2\pi}\cos\left(iu_k - a\right), \end{cases} \quad |k| \le \frac{N}{2}, \tag{15}$$

where $u_k = kh$, with an appropriate step size h. As shown in [22], selection of the parameters h, μ and a can be made by asymptotic balancing of the error terms. There will be two sources of error in the approximation: the truncation error, which arises when the infinite limits $-\infty < u < \infty$ are truncated to $|u| \le Nh/2$; and the discretization error, or quadrature error due to approximation of the integral with a finite sum. Unfortunately, it is not clear a priori what choice of N is required to ensure convergence with prescribed precision. For a value of N that is too large, evaluation of the impulse response over many values of (x,t) will be time-consuming. Additionally, we have found in practice that it is helpful to scale the quadrature nodes by either time $s = z/t$, or by the delayed time $s = z/(t - t_\infty)$, where $t_\infty = x/c_\infty$ is the arrival time of the wavefront. The correct choice of both N and the method of scaling is ultimately determined by the size of x and the time interval over which the solution is to be computed.

This construction of the impulse response $\Psi(x,t)$ will be employed to validate the asymptotic behavior of the H-N medium response at short and large depths in Section 3. Solutions obtained using this hyperbolic contour have been validated by computing the impulse response with an alternative method that first folds the Bromwich curve on the branch cut, $s = ue^{\pm\pi i}$, $0 < u < \infty$, and then discretizes the resulting integral with Gauss-Legendre quadrature and an excessively large number of nodes (3 to 4 times as many as those used in the hyperbolic contour) to ensure sufficient convergence. Also, we have employed a numerical method of known accuracy [21] to validate the numerical inverse Laplace transforms discussed above and the asymptotic results obtained below.

III. Asymptotic Analysis

We now present an asymptotic investigation of the impulse response (10) for short and large depths into the H-N dielectric half-space. The results will be presented for the general (H-N) case, but are also valid for the limiting cases of the C-C and C-D models. Section 3.2.1 will also provide the resolution of the open problem identified in [16].

A. The Wavefront Region

We first examine the wavefront after propagation over a short depth into the H-N medium characterized by $t \approx x^+/c_\infty \ll \tau$. We will also refer to this asymptotic regime in terms of the parameter (13) which satisfies $\theta \approx 1^+$ near the wavefront. If in (10) we substitute $s = z/t$ and assume $t \ll \tau$, we see that the phase of the wavefront behavior will be determined by the infinite-frequency approximation

$$q(s\tau) \approx 1 + \frac{r-1}{2}(s\tau)^{-\alpha\beta} + O\left((s\tau)^{-\alpha(\beta+1)}\right), \tag{16}$$

which is obtained by retaining the first two terms of the expansion of (8) for large $s\tau \gg 1$. Inserting (16) into (10), the leading order behavior of the impulse response at the wavefront is then obtained as $\Psi(x,t) \approx \Psi_\infty(x,t)$, where

$$\Psi_\infty(x,t) = \frac{1}{2\pi i}\int_{\zeta-i\infty}^{\zeta+i\infty} e^{s\left(t - \frac{x}{c_\infty}\right)} e^{-Ax(s\tau)^{1-\alpha\beta}} ds, \tag{17}$$

with $A = \frac{(r-1)}{2c_\infty\tau}$. The integrand in (17) is written in a factored form in order to distinguish between two prominent features of the early impulse response. The argument of the first exponential factor is a hyperbolic term, which shows that the wavefront will propagate with the infinite-frequency speed c_∞. The second exponential factor will act as a smoothing operator on the incoming pulse. Notice that the parameters α and β only appear as a product $\alpha\beta$ in this approximation; thus the behavior of the electric field in the skin-depth cannot be distinctly discerned as corresponding to a C-C, C-D, or H-N medium, unless other considerations have determined that $\beta < 1$.

To elaborate on the smoothing effects of the early impulse response, we compute the early wavefront response for the electric field due to an incident pulse $f(t)$ by first taking the Laplace transform

$$\mathcal{L}[\Psi_\infty] = \hat{\Psi}_\infty(x,s) = e^{-\frac{sx}{c_\infty} - Ax(s\tau)^{1-\alpha\beta}}, \tag{18}$$

differentiating with respect to x, and inverting the resulting expression to produce the governing equation for the effective short depth impulse response

$$\frac{1}{c_\infty}\frac{\partial \Psi_\infty}{\partial t} + \frac{\partial \Psi_\infty}{\partial x} = -A(\tau D_t)^{1-\alpha\beta}\Psi_\infty, \qquad (19)$$

where the right hand side is a fractional derivative, and acts as a smoothing operator for $\alpha\beta < 1$. Thus

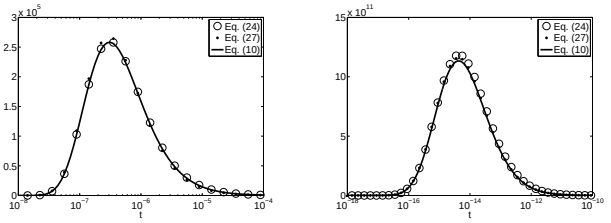

(a) $\alpha\beta = 0.45$ (b) $\alpha\beta = 0.8$

Figure 2: Validation of the infinite-frequency approximation of the Havriliak-Negami impulse response, at $x = 0.0002 c_\infty \tau$. The time is translated, so that the origin is at $t = \frac{x}{c_\infty}$.

$E(x,t)$ will be infinitely smooth for $\alpha\beta < 1$ since

$$\lim_{t\to x^+/c_\infty} \frac{\partial^n E}{\partial t^n} = \lim_{s\to+\infty} s^n \hat{E}(x,s)$$
$$= \lim_{s\to+\infty} s^n F(s) e^{-Axs^{1-\alpha\beta}} = 0 \qquad (20)$$

for $n \geq 0$. This result was shown in [16] to hold for the C-C model, and now it can be seen to generalize to the H-N and C-D models. In the limit $\alpha\beta \to 1$, the behavior in a Debye medium is recovered, and the solution of (19) will be $E(x,t) \approx f(t - x/c_\infty)e^{-Ax}$, which shows $E(x,t)$ will not be infinitely smooth at the wavefront and will now inherit any discontinuities in the signal $f(t)$.

In contrast to the exact impulse response discussed in Section 2, the short-depth approximation Ψ_∞ can be successfully computed using the method of steepest descents. This is due to the simpler expression for the phase, which can be used to obtain a closed form representation of the contour. The saddle point is now obtained by setting $d\phi/ds = 0$, where $\phi = s(t - x/c_\infty) - Ax(s\tau)^{1-\alpha\beta}$ is the phase of (17). This results in

$$s^* = \frac{1}{\tau}\left(\frac{(1-\alpha\beta)Ax}{t - x/c_\infty}\right)^{\frac{1}{\alpha\beta}}$$
$$= \frac{1}{\tau}\left(\frac{1-\alpha\beta}{2}\left(\frac{r-1}{\theta-1}\right)\right)^{\frac{1}{\alpha\beta}} \qquad (21)$$

Notice that we have a moving saddle point, as it is inversely proportional to $(\theta - 1)$; thus we first make the change of variables $s\tau = z\lambda$ in equation (17), where $\lambda = (\theta-1)^{-1/\alpha\beta}$ will be a large positive parameter (recall that $\theta = c_\infty t/x \approx 1$ at the wavefront). This will ensure that the main contribution of the integral will remain localized near the saddle point, which is now given as $z^* = ((1-\alpha\beta)(r-1)/2)^{\frac{1}{\alpha\beta}}$ and is stationary. Making this change of variables in (17) produces

$$\Psi_\infty = \frac{\lambda}{2\pi i\tau}\int_{\zeta-i\infty}^{\zeta+i\infty} e^{\lambda\left(\frac{t}{\tau} - \frac{x}{c_\infty\tau}\right)\left(z - \frac{r-1}{2}z^{1-\alpha\beta}\right)} dz. \qquad (22)$$

After substituting the second order approximation of the phase about $z = z^*$,

$$\phi \approx -\frac{\alpha\beta x\lambda^{1-\alpha\beta}z^*}{(1-\alpha\beta)c_\infty\tau}\left(1 - \frac{1-\alpha\beta}{2}\left(\frac{z}{z^*} - 1\right)^2\right), \qquad (23)$$

we integrate the resulting expression to obtain the leading order term of the asymptotic series,

$$\Psi_\infty \approx \frac{1}{\tau}\sqrt{\frac{z^*\lambda c_\infty\tau}{2\pi\alpha\beta(c_\infty t - x)}}\, e^{-\frac{\alpha\beta\lambda z^*}{1-\alpha\beta}\left(\frac{t}{\tau} - \frac{x}{c_\infty\tau}\right)}, \qquad (24)$$

which is valid to $O(1/\lambda)$. Figure 2 shows the saddle point approximation for $x = 0.0002 c_\infty\tau, r = 75$, and $\alpha\beta = 0.45, 0.8$ respectively, compared to the exact impulse response, obtained using the hyperbolic Bromwich contour (14) to evaluate (10). We also show the result of numerically evaluating (17) along the steepest descent contour, computed as detailed below. Note that the relative amplitude of the impulse response depends strongly on $\alpha\beta$, and approaches infinity for $\alpha\beta = 1$; this reflects the fact that $\Psi_\infty = \delta(t - x/c_\infty)e^{-Ax}$ for the Debye response. Additionally, note that the approximations show better agreement with the exact response for smaller $\alpha\beta$; this is because λ will be larger for smaller $\alpha\beta$, which makes the saddle point approximation (24) more accurate. In Figure 3 we show the result of convolving (24) with signaling data consisting of a unit-amplitude rectangular pulse of duration τ.

In order to directly evaluate (17), as shown in Figure 2, we first find a parametric representation of the steepest descent contour. This is most easily accomplished in polar form. We first define $s\tau = \rho e^{i\sigma}$, and then note from equation (21) that both s^*

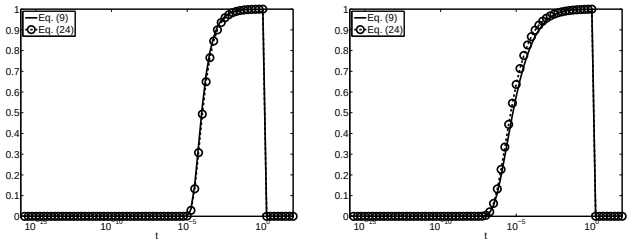

(a) $\alpha\beta = 0.45$ (b) $\alpha\beta = 0.8$

Figure 3: Time-domain response with rectangular-pulse signaling data, recorded at $x = 0.0002 c_\infty \tau$. The time is translated, so that the origin is at $t = \frac{x}{c_\infty}$.

and $\phi(s^*)$ will be real, so that the steepest descent contour satisfies $\Im[\phi] = 0$. This leads to

$$\rho(\sigma) = s^* \left[\frac{\sin\left((1-\alpha\beta)\sigma\right)}{(1-\alpha\beta)\sin\sigma} \right]^{\frac{1}{\alpha\beta}}, \quad |\sigma| \le \pi. \quad (25)$$

For the sake of simplicity, we define the function

$$S(\sigma; a, b) = \frac{b \sin(a\sigma)}{a \sin b\sigma}, \quad S(0; a, b) = 1 \quad (26)$$

so that $\rho(\sigma) = s^* S(\sigma; 1-\alpha\beta, 1)^{1/\alpha\beta}$, and $\rho(0) = s^*$. This contour is shown in Figure 4 for comparison to Figure 1. The contours are only of interest for $\theta \approx 1^+$, since this is where the approximation (17) is asymptotically valid. Using the parametric

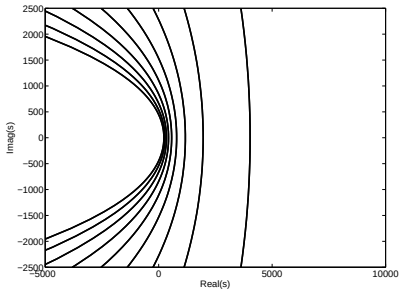

Figure 4: Steepest descent contour for the phase of the short-depth approximation of the H-N impulse response (17). Contours are shown for $1 < \theta \le 3$, since the asymptotic regime corresponds to $\theta \approx 1^+$.

representation and the expression (26), the short-depth approximation of the impulse response takes the form

$$\Psi_\infty = \frac{1}{2\pi\tau} \int_{-\pi}^{\pi} e^{-\alpha\beta\left(\frac{t}{\tau} - \frac{x}{c_\infty \tau}\right)\rho S(\sigma;\alpha\beta,1)} \times \rho S(\sigma; \alpha\beta, 1-\alpha\beta) d\sigma. \quad (27)$$

Approximation of this integral can be accomplished using the trapezoidal rule, which yields exponential convergence,

$$\Psi_\infty = \sum_{k=-N}^{N} w_k e^{-\alpha\beta\left(\frac{t}{\tau} - \frac{x}{c_\infty \tau}\right)\rho_k S_k(\alpha\beta,1)}, \quad (28)$$

where $\rho_k = \rho(\sigma_k)$, and

$$w_k = \frac{\rho_k S_k(\alpha\beta, 1-\alpha\beta)}{2(N+1)\tau}, \quad \sigma_k = \frac{k\pi}{N+1}.$$

B. The Large-depth Behavior

We now examine the behavior of the propagating pulse at depths satisfying $x \gg c_\infty \tau$. In this region, we will take $t \approx x/c_s > \tau$, or alternatively $\theta \approx c_\infty/c_s$. This regime corresponds to the $|s\tau| \ll 1$ limit of (8); an asymptotic expansion yields

$$q(s\tau) \approx \sqrt{r} - \beta \frac{r-1}{2\sqrt{r}} (s\tau)^\alpha + O\left((s\tau)^{2\alpha}\right), \quad (29)$$

where $\sqrt{r} = c_\infty/c_s$. The leading order large-depth approximation of the impulse response is $\Psi(x,t) \approx \Psi_0(x,t)$, where

$$\Psi_0(x,t) = \frac{1}{2\pi i} \int_{\zeta - i\infty}^{\zeta + i\infty} e^{s\left(t - \frac{x}{c_s}\right)} e^{Bx(s\tau)^{1+\alpha}} ds, \quad (30)$$

with $B = \beta \frac{r-1}{2rc_s\tau}$.

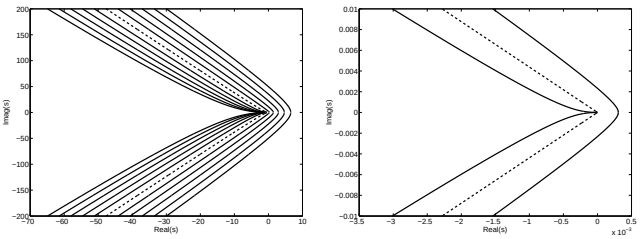

(a) Zoom-out (b) Zoom-in

Figure 5: Steepest descent contour of the large-depth approximation, with increasing values of θ. The separatrix (dotted line) is given by $s = \rho e^{\pm\pi i/(1+\alpha)}$, $\rho > 0$, and corresponds to $\theta = c_\infty/c_s$.

To accomplish the evaluation of $\Psi_0(x,t)$, we again compute the inverse Laplace transform along a steepest descent contour in the complex $s-$domain.

Now the phase is $\phi = s\left(t - \frac{x}{c_s}\right) + Bx(s\tau)^{1+\alpha}$ and the saddle point will be

$$\begin{aligned} s^* =& \frac{1}{\tau}\left(\frac{1-\frac{c_s t}{x}}{\beta\frac{r-1}{2r}(1+\alpha)}\right)^{\frac{1}{\alpha}} \\ =& \frac{1}{\tau}\left(\frac{1-\frac{\theta}{\sqrt{r}}}{1+\alpha}\frac{2r}{\beta(r-1)}\right)^{\frac{1}{\alpha}}. \end{aligned} \tag{31}$$

From this expression, we see that for $t < x/c_s$ the saddle point will be real which will make the phase real as well. We first make the change of variables $s\tau = \lambda z$, with $\lambda = (1-\theta/\sqrt{r})^{1/\alpha}$; after substituting the second order approximation of the phase about $z = z^*$ we have

$$\phi \approx -\frac{\alpha x \lambda^{1+\alpha} z^*}{(1+\alpha)c_s\tau}\left(1 + \frac{1+\alpha}{2}\left(\frac{z}{z^*}-1\right)^2\right), \tag{32}$$

where $z^* = (\beta(1-\alpha)(r-1)/2r)^{-1/\alpha}$, and thus

$$\Psi_0 \approx \frac{1}{\tau}\sqrt{\frac{z^*\lambda c_s\tau}{2\pi\alpha(x-c_s t)}}e^{-\frac{\alpha}{1+\alpha}z^*\lambda\left(\frac{x}{c_s\tau}-\frac{t}{\tau}\right)}, \tag{33}$$

up to $O(1/\lambda)$. Clearly, (33) loses validity as $t \to (x/c_s)^-$ since $\lambda \to 0$ and the asymptotic series diverges thus rendering the leading order term useless for $t \geq x/c_s$. This issue was identified in [16] as an open problem and to resolve it we evaluate (30) by finding a parametric form of the steepest descent contour, as in the case of the shallow-depth response, and discretize the resulting integral. By setting $s\tau = \rho e^{i\sigma}$, and setting the imaginary part of the phase to zero, we obtain the parametric form

$$\rho(\sigma) = s^* S(\sigma; 1, 1+\alpha)^{\frac{1}{\alpha}}, \quad |\sigma| \leq \frac{\pi}{1+\alpha}, \tag{34}$$

where the $S(\sigma; a, b)$ is again given by (26), and the interval is taken to ensure that the expression remains real for $t < x/c_s$. Note that this expression satisfies $\rho(0) = s^*$. We note here that this calculation agrees with (33) in the time interval where it is valid (see Figure 7).

At $t = x/c_s$ (30) can be evaluated analytically. Now, the saddle point vanishes, and the expression (34) is no longer valid; the phase simplifies to $\phi = Bx(s\tau)^{1+\alpha}$, which can be made real along the rays $\arg s = \pm\pi/(1+\alpha)$. The approximate impulse response is thus given by

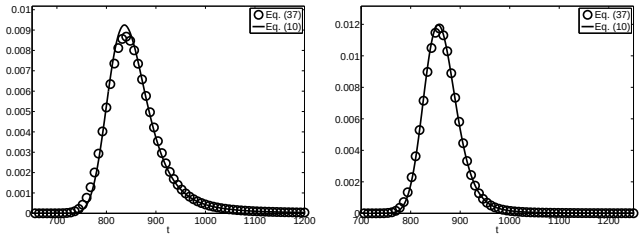

(a) $(\alpha, \beta) = (0.6, 0.75)$ (b) $(\alpha, \beta) = (0.8, 0.75)$

Figure 6: Validation of the large-depth approximation of the H-N Impulse Response at $x = 100c_\infty\tau$.

$$\begin{aligned} \Psi_0|_{t=x/c_s} &= \frac{1}{2\pi i}\int_{\zeta-i\infty}^{\zeta+i\infty} e^{Bx(s\tau)^{1+\alpha}} ds \\ &= \frac{e^{\gamma\pi i} - e^{-\gamma\pi i}}{2\pi i}\int_0^\infty e^{-Bxv^{1+\alpha}} dv \\ &= \frac{\sin(\pi\gamma)}{\pi}(Bx)^{-\gamma}\int_0^\infty e^{-v^{1+\alpha}} dv \\ &= \frac{\gamma(Bx)^{-\gamma}}{\Gamma(\gamma)\Gamma(1-\gamma)}\int_0^\infty e^{-u}u^{\gamma-1} du \\ &= \frac{\gamma(Bx)^{-\gamma}}{\Gamma(1-\gamma)}, \end{aligned} \tag{35}$$

where $\gamma = \frac{1}{1+\alpha}$, and we have used the identity $\Gamma(1-z)\Gamma(z) = \pi/\sin(\pi z)$.

When $t > x/c_s$, the saddle point vanishes, since it passes into the branch cut on the negative real $s-$axis; however the same expression (34) will still define a steepest descent contour. It is merely the domain that must be changed, which is instead comprised of the disjoint intervals defined by $\pm\sigma \in (\pi/(1+\alpha), \pi)$. On these intervals, $\sin((1+\alpha)\sigma)$ is negative, which in turn makes $S(\sigma; 1, 1+\alpha)$ negative; but this sign change is compensated by an additional change in the numerator of s^* due to $1 - c_s t/x$, and therefore the parametric representation remains real. The two disjoint intervals in σ form a cusp at the origin in the complex s domain, which corresponds to $\rho(\pm\pi) = 0$. The two regimes, namely that with the saddle point, and that with the cusp, are separated by the steepest descent contour along which $t = x/c_s$, as is shown in Figure 5. This latter curve will be comprised of the two rays $s\tau = \rho e^{\pm\pi i/(1+\alpha)}$, and must therefore be treated separately. Note that this behavior in the steepest descent contours is similar to those of the exact impulse response, shown in Figure 1.

We can now express the approximate impulse response for $t \neq x/c_s$ by replacing $s\tau = \rho(\sigma)e^{i\sigma}$, and retaining the real part of the resulting integral; the imaginary part is odd with respect to the imaginary axis, and will therefore vanish. After some manipulation, we obtain

$$\Psi_0 = \frac{1}{2\pi\tau}\int e^{\alpha\left(\frac{t}{\tau}-\frac{x}{c_s\tau}\right)\rho S(\sigma;\alpha,1)}\times \rho S(\sigma;\alpha,1+\alpha)d\sigma, \tag{36}$$

where the endpoints are chosen depending on the sign of $t - x/c_s$. This integral can be approximated with exponential accuracy using the trapezoidal rule,

$$\Psi_0 \approx \sum_{k=-N}^{N} w_k e^{\alpha\left(\frac{t}{\tau}-\frac{x}{c_s\tau}\right)\rho_k S_k(\alpha,1)}, \tag{37}$$

where $\rho_k = \rho(\sigma_k)$,

$$\sigma_k = \begin{cases} \frac{k}{N}\frac{\pi}{1+\alpha}, & t < \frac{x}{c_s} \\ \pi - \frac{k}{N}\frac{\alpha\pi}{1+\alpha}, & t > \frac{x}{c_s}, \end{cases} \tag{38}$$

and

$$w_k = \frac{1+\alpha}{2N\alpha\tau}\begin{cases} \alpha\rho_k S_k(\alpha,1+\alpha), & t < \frac{x}{c_s} \\ \rho_k S_k(\alpha,1+\alpha), & t > \frac{x}{c_s}. \end{cases} \tag{39}$$

The approximate impulse response is compared

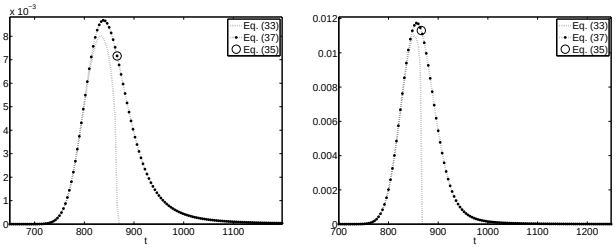

(a) $(\alpha, \beta) = (0.6, 0.75)$ (b) $(\alpha, \beta) = (0.8, 0.75)$

Figure 7: Validation of (33) and (35) at $x = 100c_\infty\tau$.

in Figure 6 for the same parameters as Figure 2 but for $x = 100c_\infty\tau$. Once again, the hyperbolic contour (14) is used to evaluate the exact impulse responses Ψ. As illustrated in Figure 6, the approximate impulse response clearly improves as α increases, but in both cases the peak of the exact impulse response is slightly underestimated. The saddle point approximation is not shown, since it does not provide an accurate approximation for $t \geq x/c_s$. However, Figure 7 shows the correctness of (35), and the accuracy of (33) when it is valid. The splicing of (33), (35), and (37) provides the resolution of the open problem identified in [16].

IV. Applications

A. Time-Domain Reflectometry

We now discuss the possible application of the results obtained in Section 3 to perform medium-model parameter estimation using recorded propagating pulses in TDR experiments. In [2], it was shown in the case of the Debye model that for large depths the electric field satisfies an advection-diffusion equation with the zero-frequency subcharacteristic speed c_s. This results in a symmetric response, whose peak is located on the subcharacteristic ray $t = x/c_s$. But in the C-C model [16], the peak was found not to coincide with this ray; rather, it is the mean electric field that does. When $\alpha \to 1^-$, the peak and mean electric fields coalesce. More importantly, we can compute the time at which the mean electric field occurs using the mean value theorem,

$$\bar{t}(x) = \frac{\int_0^\infty t' E(x,t')dt'}{\int_0^\infty E(x,t')dt'}.$$

Upon constructing this quantity, we find that $\bar{t}$ is a linear function of x, with slope $1/c_s$. The intercept can be computed by setting $x = 0$, and doing so provides an alternate expression in terms of the incident pulse

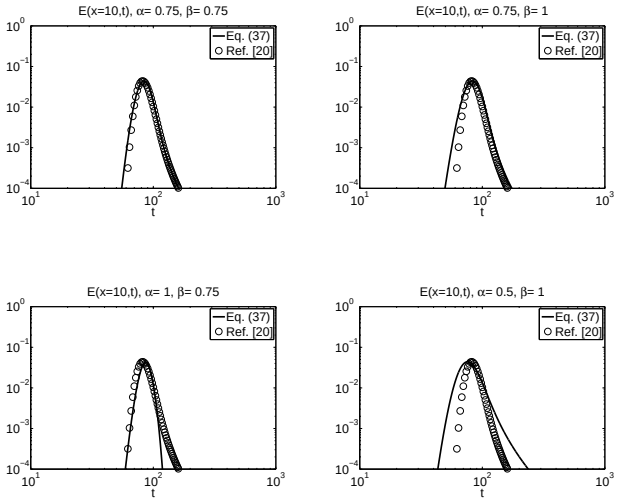

Figure 8: Log-log plots comparing late asymptotic approximation to a numerical solution with $\alpha = \beta = 0.75$.

$$\bar{t}(x) = \bar{t}(0) + \frac{x}{c_s} = \frac{\int_0^\infty t' f(t')dt'}{\int_0^\infty f(t')dt'} + \frac{x}{c_s}. \tag{40}$$

Note that if we have an experimentally obtained (which is herein simulated with our method in [21]) time trace that is recorded at a known x location, we can approximate $\bar{t}$. By setting the two expressions equal, we can then isolate the subcharacteristic speed and in turn obtain ϵ_s

$$\epsilon_s = \frac{(\bar{t}(x) - \bar{t}(0))^2}{x^2 \epsilon_0 \mu_0}.$$

This provides for a straightforward way to compute this model parameter without fitting.

The late asymptotic response (37) may be used to determine the parameters α and β of the H-N model. In figure 8 a numerical solution [21] represents a "measured" electric field, in an H-N model with $\alpha = \beta = 0.75$, that is meant to represent a TDR data set, and is plotted on a log-log scale. The first plot (upper left panel) shows the fit when the correct parameters are chosen in (37); the responses to the right of the peak exactly match. Note that when the correct value of α is found, but β is not correct, the curves to the right of the peak are identical apart from a constant-in-time offset whose magnitude is controlled by β (top right panel). In both lower panels, the value of α is incorrect, and we can clearly see that the curves are not parallel in the region to the right of the peak. This is true even in the lower left panel, where β is correct. Thus, we can first determine α by fitting (37) to data measured at times after the arrival of the peak of the response for any value of β (to produce a situation as shown in the upper right panel of figure 8), and then adjust β until we have the agreement shown in the upper left panel of figure 8. Finally, (24) and (35) could be used with measured propagating pulse data at small depths to provide two equations from which the remaining parameters of (1), ϵ_∞ and τ, can be inferred from.

B. Fractional Precursors and Non-Dispersive Random Media

In a recent publication [23], sound pulse propagation in a random fluctuating acoustic medium is studied using ensemble averaging to arrive at effective fractional differential equations describing the time-dependent pressure waves. The wavefront is identified in [23] by an algebraically decaying bump, or fractional precursor, which propagates into the acoustic medium. This deterministic pulse, resulting from the underlying stochastic properties of weakly random media with short- and long-range correlations, closely resembles the H-N medium model response which we have analyzed. Indeed, we can establish a relationship between our parameters α and β, and the Hurst parameter H used in [23] as follows. By inserting equation (4) into equation (2), we obtain a partial integro-differential wave equation satisfied by the electric field,

$$\frac{\partial^2 E}{\partial x^2} - \frac{1}{c_\infty^2}\frac{\partial^2 E}{\partial t^2} = \int_0^t \frac{\chi(t-s)}{c_\infty^2}\frac{\partial^2 E(x,s)}{\partial s^2} ds. \quad (41)$$

Recalling that $\chi(t) \sim t^{\alpha\beta-1}$ as $t \to 0^+$, the asymptotically valid effective fractional differential equation is, formally, as follows

$$\frac{\partial^2 E}{\partial x^2} - \frac{1}{c_\infty^2}\frac{\partial^2 E}{\partial t^2} \approx \int_0^t \frac{(t-s)^{\alpha\beta-1}}{c_\infty^2 \Gamma(\alpha\beta)}\frac{\partial^2 E(x,s)}{\partial s^2} ds. \quad (42)$$

Equation (42) can be compared directly to (25) of [23] with appropriate scaling provided the Hurst parameter satisfies $2H = \alpha\beta \in (0,1)$. Thus, the results reported here for short depth asymptotics in the H-N dielectric model coincide with those of the short-range correlation acoustic medium problem in [23]. In the long time limit $\chi(t) \sim t^{-\alpha-1}$, and so we have, again formally,

$$\frac{\partial^2 E}{\partial x^2} - \frac{1}{c_0^2}\frac{\partial^2 E}{\partial t^2} \approx \int_0^t \frac{(t-s)^{-\alpha}}{c_0^2 \Gamma(\alpha)}\frac{\partial^3 E(x,s)}{\partial s^3} ds, \quad (43)$$

which after a suitable scaling coincides with (30) of [23] provided we identify $H = 1 + \alpha$ as the relationship between the Hurst parameter and our fractional parameters. This correspondence between our work and that of [23] opens the possibility of being able to identify statistics of actual dielectric mixtures using time-dependent waveforms recorded in TDR experiments. Figure 9 shows a computation performed by convolving the signaling data described in the caption with a numerical evaluation of our Equation (10), as described in Section II above, and suggests that the H-N model is the homogenization (in the sense of [23]) of a lossless non-dispersive random medium that exhibits both short- and long-range correlations.

REFERENCES

[1] P. Petropoulos, "The wave hierarchy for propagation in relaxing dielectrics," *Wave Motion*, vol. 21, no. 3, pp. 253–262, May 1995.

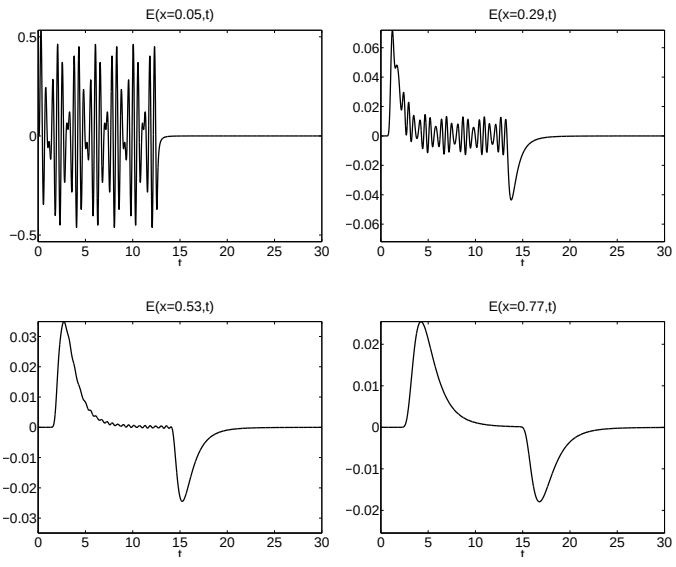

Figure 9: Time-domain response of the HN medium at four non-dimensional depths for signaling data $E(0,t) = \sin(4\pi t)\cos(\frac{\pi t}{2})H(t)$, where $H(t) = 1$ for $0 \leq t \leq 12.5$ and $H(t) = 0$ for $t > 12.5$. The medium model parameters are $\alpha = 0.8$, $\beta = 0.6$, $\epsilon_s = 50$, $\epsilon_\infty = 1$, and $\tau = 1$.

[2] T. M. Roberts and P. G. Petropoulos, "Asymptotic and energy estimates for electromagnetic pulses in dispersive media," *J. Opt. Soc. Am. A*, vol. 13, no. 6, pp. 1204–1217, 1996.

[3] M. Kelbert and I. Sazonov, *Pulses and Other Wave Processes in Fluids*. Dordrecht, The Netherlands: Kluwer Academic, 1996.

[4] T. M. Roberts and P. G. Petropoulos, "Asymptotics and energy estimates for electromagnetic pulses in dispersive media: addendum," *J. Opt. Soc. Am. A*, vol. 16, no. 11, pp. 2799–2800, 1999.

[5] P. Debye, *Polar Molecules*. New York: Dover, 1929.

[6] T. M. Roberts, "Measured and predicted behavior of pulses in debye- and lorentz-type materials," *IEEE Trans. Antennas Propag.*, vol. 52, no. 1, pp. 310–314, 2004.

[7] E. G. Farr and C. A. Frost, "Impulse propagation measurements of water, dry sand, moist sand, and concrete," *U.S. Air Force Weapons Lab., Technical Rep. WL-TR-1997-7051*, 1997.

[8] F. E. Stoudt, D. C. Peterkin and B. J. Hankla, "Transient rf and microwave pulse propagation in a debye medium (water)," *Naval Surface Warfare Center, Interaction Note 622, available from www.ece.unm.edu/summa/notes/Interaction.html*, 2011.

[9] R. Hilfer, "H-function representations for stretched exponential relaxation and non-debye susceptibilities in glassy systems," *Phys. Rev. E*, vol. 65, no. 6, pp. 061 510–061 514, Jun 2002.

[10] A. Schönhals, F. Kremer, and E. Schlosser, "Scaling of the α relaxation in low-molecular-weight glass-forming liquids and polymers," *Phys. Rev. Lett.*, vol. 67, no. 8, pp. 999–1002, Aug 1991.

[11] T. Repo and S. Pulli, "Application of impedance spectroscopy for selecting frost hardy varieties of english ryegrass," *Annals of Botany*, no. 78, pp. 605–609, 1996.

[12] P. Polk and E. Postow, *Handbook of Biological Effects of Electromagnetics Fields*. Boca Raton, Florida: CRC Press, 1995.

[13] T. Kim, J. Kim, and J. Pack, "Dispersive effect of uwb pulse on human head," Electromagnetic Compatibility, 2007. EMC Zurich 2007. 18th International Zurich Symposium on, pp. 41–44, 2007.

[14] S. Gabriel, R. W. Lau, and C. Gabriel, "The dielectric properties of biological tissues: Iii. parametric models for the dielectric spectrum of tissues," *Phys. Med. Biol.*, vol. 41, no. 11, pp. 2271–2293, 1996.

[15] W. S. Bigelow and E. G. Farr, "Impulse propagation measurements of the dielectric properties of several polymer resins," *Farr Research Inc., available as www.farr-research.com/Papers/mn55.pdf*, 1999.

[16] P. Petropoulos, "On the time-domain response of cole-cole dielectrics," *Antennas and Propagation, IEEE Transactions on*, vol. 53, no. 11, pp. 3741–3746, 2005.

[17] K. Cole and R. Cole, "Dispersion and absorption in dielectrics i. alternating current characteristics," *J. Chem. Phys.*, vol. 9, pp. 341–52, 1941.

[18] D. Davidson and R. Cole, "Dielectric relaxation in glycerol, propylene glycol, and n-propanol," *J. Chem. Phys.*, vol. 19, pp. 1484–1490, 1951.

[19] S. Havriliak and S. Negami, "A complex plane representation of dielectric and mechanical relaxation processes in some polymers," *Polymer*, vol. 8, no. 4, p. 161, 1967.

[20] Y. P. Kalmykov, W. T. Coffey, D. S. F. Crothers, and S. V. Titov, "Microscopic models for dielectric relaxation in disordered systems," *Phys. Rev. E*, vol. 70, p. 041103, 2004.

[21] M. F. Causley, P. G. Petropoulos, and S. Jiang, "Incorporating the havriliak-negami dielectric model in the fd-td method," *J. Comput. Physics*, pp. 3884–3899, 2011.

[22] J. A. C. Weideman and L. N. Trefethen, "Parabolic and hyperbolic contours for computing the bromwich integral," *Math. Comput.*, vol. 76, no. 259, pp. 1341–1356, 2007.

[23] J. Garnier and K. Solna, "Fractional precursors in random media," *Waves in Random and Complex Media*, vol. 20, no. 1, pp. 122–155, 2009.

Matthew F. Causley received the B.S. degree in applied mathematics with Honors from Kettering University, Flint, MI, in 2006 and the Ph.D. degree in mathematical sciences from the New Jersey Institute of Technology, Newark, NJ, in 2011. He is currently a Postdoctoral Investigator with the Department of Mathematics, Michigan State University, East Lansing, MI. His current research is on novel numerical methods for modeling plasmas. His research interests include computational electromagnetics, wave propagation in dispersive dielectrics, and fast convolution techniques.

Peter G. Petropoulos received the B.S.E.E. degree with Highest Honors from Rutgers University, New Brunswick, NJ, in 1986 and the Ph.D. degree in applied mathematics from Northwestern University, Evanston, IL, in 1991. From 1991 to 1994, he was a Postdoctoral Fellow with the Directed Energy Division, U.S.A.F. Armstrong Laboratory, Brooks AFB, TX, and from 1994 to 1998, he was an Assistant Professor with the Department of Mathematics, Southern Methodist University. Since 1998, he has been with the Department of Mathematical Sciences, New Jersey Institute of Technology, Newark, NJ, where he is currently an Associate Professor. His research is in the areas of wave propagation, computational electromagnetics, and microscale electrohydrodynamics.